Structural ordering and interface morphology in symmetrically strained (GaIn)As/Ga(PAs) superlattices grown on off-oriented GaAs(100)

C. Giannini, L. Tapfer, Y. Zhuang,* and L. De Caro
Centro Nazionale Ricerca e Sviluppo Materiali (PA.S.T.I.S.–C.N.R.S.M.), S.S. Appia Km. 712, Brindisi I-72100, Italy

T. Marschner and W. Stolz
Wiss. Zentrum für Materialwissenschaften und Fachbereich Physik, Philipps-Universität, Hans-Meerwein-Strasse, D-35032 Marburg, Germany

(Received 5 August 1996)

In this work we investigate the structural properties of symmetrically strained (GaIn)As/GaAs/Ga(PAs)/GaAs superlattices by means of x-ray diffraction, reciprocal-space mapping, and x-ray reflectivity. The multilayers were grown by metalorganic vapor-phase epitaxy on (001) GaAs substrates intentionally off-oriented towards one of the nearest ⟨110⟩ directions. High-resolution triple-crystal reciprocal-space maps recorded for different azimuth angles in the vicinity of the (004) Bragg diffraction clearly show a double periodicity of the x-ray peak intensity that can be ascribed to a lateral and a vertical periodicity occurring parallel and perpendicular to the growth surface. Moreover, from the intensity modulation of the satellite peaks, a lateral-strain gradient within the epilayer unit cell is found, varying from a tensile to a compressive strain. Thus, the substrate off-orientation promotes a lateral modulation of the layer thickness (ordered interface roughness) and of the lattice strain, giving rise to laterally ordered macrosteps. In this respect, contour maps of the specular reflected beam in the vicinity of the (000) reciprocal lattice point were recorded in order to inspect the vertical and lateral interface roughness correlation. A semiquantitative analysis of our results shows that the interface morphology and roughness is greatly influenced by the off-orientation angle and the lateral strain distribution. Two mean spatial wavelengths can be determined, one corresponding exactly to the macrostep periodicity and the other indicating a further interface waviness along the macrosteps. The same spatial periodicities were found on the surface by atomic-force-microscopy images confirming the x-ray results and revealing a strong vertical correlation of the interfaces up to the outer surface. [S0163-1829(97)10407-6]

I. INTRODUCTION

The surface morphology of a growing film is mainly controlled by surface kinetic processes, i.e., nucleation, diffusion, chemisorption, etc. Besides these processes, recent studies on strained structures revealed the fundamental role of the strain in determining the growth morphology.[1–5] Furthermore, changes in surface roughness have been reported as a function of the sign of the strain incorporated in the material systems: a surface flattens under tensile strain while it becomes rough under compressive strain.[6] The discovery of this relationship offered the possibility of tailoring the surface morphology of strained structures by changing the incorporated strain. In fact, strained induced growth of lateral periodic strained superlattices has been already demonstrated for symmetrically strained multilayers.[7,8] Moreover, symmetrically strained multilayers form surface macrosteps if grown on off-oriented substrates.[9]

In this context, with this work we intend to give an accurate structural description of (GaIn)As/Ga(PAs) symmetrically strained superlattices grown by metalorganic vapor-phase epitaxy (MOVPE) on a (001) GaAs substrate intentionally off-oriented towards one of the nearest ⟨110⟩ directions. In order to get a complete analysis of the structural ordering of the investigated samples different x-ray scattering methods were used: high-resolution x-ray diffraction (HRXRD), reciprocal-space mapping (RSM), x-ray specular reflectivity (XSR), and x-ray diffuse scattering (XDS). In addition, we used atomic-force microscopy (AFM) to reveal the surface morphology. HRXRD and high-angle RSM measurements were employed in order to investigate the long-range ordering of the structures along the growth direction as well as in the interface plane and for evaluating the strain distribution within the superlattice unit cell. Low-angle RSM, XSR, and XDS measurements and AFM images were recorded in order to investigate the interface and surface roughness of the superlattice and the roughness correlation among all the interfaces. Our results show a remarkably regular laterally periodic structure induced by a lateral modulation of the layer thickness and of the lattice strain. Moreover, a correlated interfacial roughness anisotropy is present that depends on the misorientation of the substrate and on the structural lateral organization of the multilayer.

II. EXPERIMENTAL DETAILS

The samples were grown by MOVPE using a commercial system equipped with a horizontal reactor (Aix 200, Aixtron Corporation) working at a pressure of 100 mbar for a growth temperature of 650 °C. The standard precursors trimethylgallium (TMGa), trimethylaluminium (TMA1), and solution trimethylindium (TMIn, Billiton precursors) were used in combination with AsH_3 and PH_3. The (001) GaAs substrates were off-oriented towards one of the nearest ⟨110⟩ directions depending on the sample, as reported in Table I. The inves-

0163-1829/97/55(8)/5276(8)/$10.00 © 1997 The American Physical Society

TABLE I. Nominal and x-ray determined values of the geometrical parameters of the investigated structures: No. is the number of periods, α is the angle between surface normal **n** and [001] direction, Λ is the period of the superlattice along the growth direction. The tensile and compressive nominal strains within the (GaIn)As and Ga(PAs) ternary compounds are given by $\pm\varepsilon$. The angle ϕ is the angle between macrosteps developing direction **r** and the equivalent $\langle 110\rangle$ direction. The lateral periodicity is indicated by L. The equivalent $\langle 110\rangle$ direction indicates the off-orientation direction of the substrate.

	Nominal				X ray				
Sample	No.	α (deg)	Λ (nm)	ε	α(deg)	Λ (nm)	ϕ (deg)	L (nm)	$\langle 110\rangle$
A	50	1.7	21.4	$\pm 10^{-2}$	2.5±0.5	20.7±0.3	48±1	330±10	[011]
B	50	1	21.4	$\pm 10^{-2}$	1.5±0.5	21.3±0.3	31±1	264± 6	[110]
C	50	2	21.4	$\pm 10^{-2}$	3 ±1	20.1±0.3	57±3	390±30	[110]
D	50	4	21.4	$\pm 10^{-2}$	6 ±2	22.2±0.3	56±4	270±30	$[0\bar{1}\bar{1}]$

tigated samples consisted of 50 periods of a [9 nm (GaIn)As]/(1.7 nm GaAs)/[9 nm Ga(PAs)]/(1.7 nm GaAs) superlattice with various lattice strains (Table I). The GaAs intralayers were deposited in order to avoid intermixing at the interface between the ternary compounds. A buffer layer composed of 10 periods of [3 nm (AlGa)As]/(3 nm GaAs) superlattice was deposited before the growth of the multilayer. Further details about the growth procedure are given in Ref. 10.

The experimental setup for double-crystal x-ray diffraction measurements (HRXRD) and high-angle reciprocal-space mappings (RSM) is equipped with a conventional 3-kW generator and a fine focus Cu-target (Cu $K\alpha$ radiation source). A four-crystal channel-cut Ge(220) crystal is used as monochromator and collimator. The x-ray beam impinging on the sample surface has a divergence of 12 sec of arc and the wavelength dispersion is estimated to be 2.5×10^{-5}. For the high-angle reciprocal-space mappings a two-crystal channel-cut Ge(220) crystal is used as an analyzer. The diffracted x-ray intensity is measured by a proportional counter (Philips MRD).

The low-angle contour maps together with the XSR and XDS measurements were performed by using a Philips-1880 diffractometer equipped with a 3-kW generator. A Cu target is used as x-ray source (Cu $K\alpha$ radiation). The x-ray beam incident on the sample is collimated by a 1/30° slit. The reflected beam is collimated by a Soller slit and by 0.1-mm receiving slit located at a distance of 100 mm from the sample, followed by a flat graphite monochromator that reflects the diffracted beam into a proportional counter.

The AFM images were obtained by using a Park Scientific Instruments microscope (BD2-210) working in air at room temperature. A piezoelectric transducer element (PZT scanner) with a maximum x-y extension (calibrated z displacement) of $10\times 10\ \mu m^2$ was used for the sample movement and a Si_3N_4 pyramidal tip of elastic constant 0.37 N/m was employed to probe the samples surface.

III. X-RAY SCATTERING METHODS

Reciprocal-space maps are isointensity contour maps recorded around a reciprocal lattice point (rlp) and plotted in a two-dimensional projection.[11] For all the RSM reported in Sec. IV the x axis corresponds to the [001] crystallographic direction and the y axis to one of the $\langle 110\rangle$ directions. For the high-angle RSM the origin of the axes coincides with the GaAs(004) rlp and for the low-angle RSM the origin corresponds to the (000) rlp.

Several important structural and geometrical parameters can be determined by a careful analysis of the high-angle RSM. The lattice periodicity along the surface normal Λ as well as the lateral periodicity L are related to the corresponding average angular distances between satellites $\Delta\omega_\Lambda$ and $\Delta\omega_L$ respectively, by[12]

$$\Lambda=\frac{|\gamma_h|\lambda}{\sin(2\theta)\Delta\omega_\Lambda},\qquad L=\frac{\cos(\theta_e)\lambda}{\sin(2\theta)\Delta\omega_L}, \tag{1}$$

where λ is the x-ray wavelength and θ is the kinematical Bragg angle. The factor γ_h is the direction cosine and the angle θ_e is the angle between the crystal surface and diffraction plane. From the alignment of satellite peaks with respect to the crystallographic axes any angle that occurs between the real structure of the epitaxial layer and the crystallographic axes can be determined, as will be demonstrated in Sec. IV A.

Specular and off-specular (longitudinal diffuse scan) reflectivity measurements (XSR) are intensity curves recorded below and above the critical angle by a coupled sample detector ω-2θ movement, where $\omega=\theta\pm\theta_{\rm off}$.[13,14] The offset angle $\theta_{\rm off}$ is zero only for the specular reflectivity curve. This measurement geometry allows a variation of the scattering vector mainly perpendicular to the sample surface plane and, for this reason, is particularly indicated to probe the structural ordering along the surface normal.

The transverse scan or diffuse scattering measurement (XDS) is performed by rocking only the sample around a specular peak and keeping the detector position fixed (2θ fixed). In this case the variation of the scattering vector occurs mainly in the sample surface plane. Therefore, transverse scans are used to investigate the in-plane structure, i.e., the structural ordering, parallel to the sample surface.[15] In order to determine the in-plane periodicity L from the XDS measurements, we reported each transverse scan recorded at the detector position $(2\theta_0)/2$, in reciprocal-space coordinates (Q_z,Q_x) where[11]

TABLE II. Nominal and x-ray determined values of the thicknesses d and lattice mismatch ε of sample A. The x-ray values are obtained from the computer simulation of the experimental double-crystal HRXRD pattern (Fig. 5) considering four subcells [see Fig. 4(c)].

	$In_xGa_{1-x}As$	GaAs	$GaP_{1-x}As_x$	GaAs	$In_xGa_{1-x}As$	GaAs	$GaP_{1-x}As_x$	GaAs
ε (10^{-2})			I				II	
Nominal	1.00	0.00	−1.00	0.00	1.00	0.00	−1.00	0.00
X-ray	0.93	0.00	−1.29	0.00	0.96	0.00	−1.15	0.00
d (nm)								
Nominal	9	1.7	9	1.7	9	1.7	9	1.7
X-ray	10.1	1.5	6.5	2.5	7.6	1.9	7.5	3.6
			III				IV	
ε (10^{-2})								
Nominal	1.00	0.00	−1.00	0.00	1.00	0.00	−1.00	0.00
X-ray	1.09	0.00	−1.19	0.00	1.18	0.00	−1.30	0.00
d (nm)								
Nominal	9	1.7	9	1.7	9	1.7	9	1.7
X-ray	7.2	1.6	10.3	1.5	7.6	2.4	8.2	2.4

$$Q_z=\frac{4\pi}{\lambda}\sin\theta_0\cos(\omega-\theta_0),$$
$$Q_x=\frac{4\pi}{\lambda}\sin\theta_0\sin(\omega-\theta_0). \tag{2}$$

In this way, the separation between satellite peaks (ΔQ_x) is directly related to the lateral lattice periodicities L by the equation

$$\Delta Q_x=\frac{2\pi}{L}. \tag{3}$$

IV. EXPERIMENTAL RESULTS AND DATA ANALYSIS

A. HRXRD and high-angle RSM measurements

Strain and geometrical parameters of the investigated superlattices were determined by means of HRXRD and RSM measurements. In particular, the geometrical parameters have been reported in Table I for all the samples (A, B, C, and D) and the strain content of a representative multilayer (sample A) is analyzed in detail (Table II).

Figure 1 shows four HRXRD measurements recorded in the vicinity of the (004) Bragg reflection in different azimuth angles around the surface normal (Ψ) for one sample, which is off-oriented towards the [011] direction (sample A). Each profile contains the substrate peak (S), the buffer and cap layer peak (B), and the superlattice satellite peaks (SL_i). The zero order is apparently missing: in fact it coincides with the substrate peak as expected for zero net strain structures. However, the presence of a miscut induces very pronounced differences of the diffraction profile recorded for different azimuth angles. Each superlattice satellite peak is composed of several peaks whose number and relative intensity changes with the azimuth angle. In order to understand this behavior we performed high-angle RSM analyses around the (004) rlp in two main azimuthal orientations of the sample.

Figure 2 shows a schematic diagram of the measurement geometry for two principal azimuthal orientations. In Figs. 2(a) and 2(b) the x-ray scattering geometry corresponds to the sample oriented in such a way that the plane containing the substrate miscut direction is parallel and perpendicular to the diffraction plane, respectively. The measurement geometries of Figs. 2(a) and 2(b) correspond to the azimuthal positions $\Psi=\pi/2$ rad and $\Psi=0$ rad, respectively. In the following, we will not specify the measurement geometry assuming that all the figures marked with (a) and (b) refer to Fig. 2(a) and Fig. 2(b), respectively, unless stated otherwise.

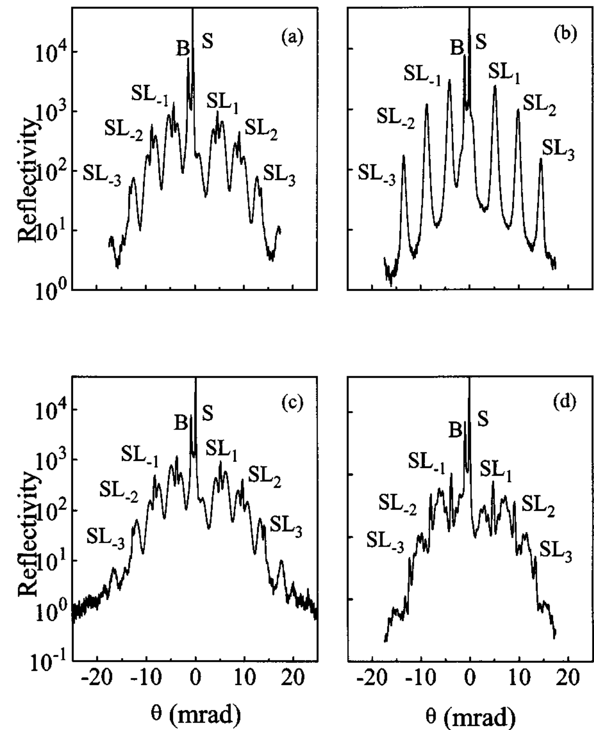

FIG. 1. Double-crystal HRXRD patterns recorded on sample A in the vicinity of the (004) Bragg reflection for different azimuth angles Ψ (rotation around the surface normal), namely, (a) $\Psi=0$ rad, (b) $\Psi=\pi/2$ rad, (c) $\Psi=\pi$ rad, and (d) $\Psi=-\pi/2$ rad.

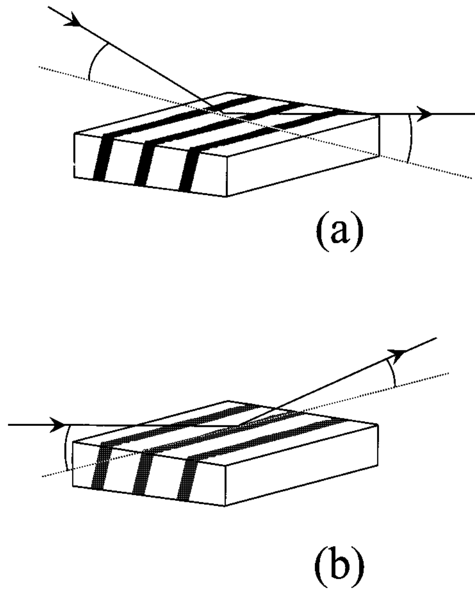

FIG. 2. Schematic diagram of the measurement geometry for two principal azimuthal orientations. The cases (a) and (b) refer to the sample orientation where the plane containing the substrate miscut direction is parallel and perpendicular to the diffraction plane, respectively. The black stripes indicate the lateral periodicity.

Figure 3 shows the RSM's collected for $\Psi=\pi/2$ rad and $\Psi=0$ rad, respectively. Our data show that if the sample is oriented as in Fig. 2(a), the experimental pattern contains the diffraction peaks due to the periodicity Λ along the growth direction together with several laterally separated diffraction spots, which can be attributed to a lateral periodicity L. This lateral periodicity disappears if the sample is rotated by $\pi/2$ around the azimuth as shown in Fig. 2(b). Therefore, it follows that the lateral periodic structure is oriented perpendicular to the miscut direction. The line connecting the satellites peaks, due to the periodicity Λ, is the actual surface normal (**n**). An angle α between the exact [001] crystallographic direction and the surface normal **n** occurs. On the contrary, the line connecting the lateral satellites peaks forms an angle ϕ with the [001] direction. A schematic description of the map is given in Fig. 4(a), where full and open circles correspond to vertical and lateral satellite peaks, respectively. The corresponding structure in the real space is shown in Fig. 4(b).

The laterally ordered thickness modulations (surface macrosteps) induce a periodic strain modulation along one surface direction. The macrosteps develop along the direction **r** which forms an angle ϕ with the [011] direction. Here, for reason of clarity the 1.9 nm thick GaAs intralayers at the interfaces are not shown. The values measured for Λ, L, α, and ϕ are reported in Table I for all the investigated samples.

The RSM shown in Fig. 3(b) contains further information about the actual structure of the sample. A complex hidden intensity distribution is observed around each Bragg satellite peak. In order to show these fine structure in more detail, double-crystal HRXRD measurements were performed for the same sample position ($\Psi=0$ rad) and almost in the same angular range (Fig. 5). Each satellite peak is actually composed of four peaks of different intensity (two of them very close to each other). The angular distance between similar

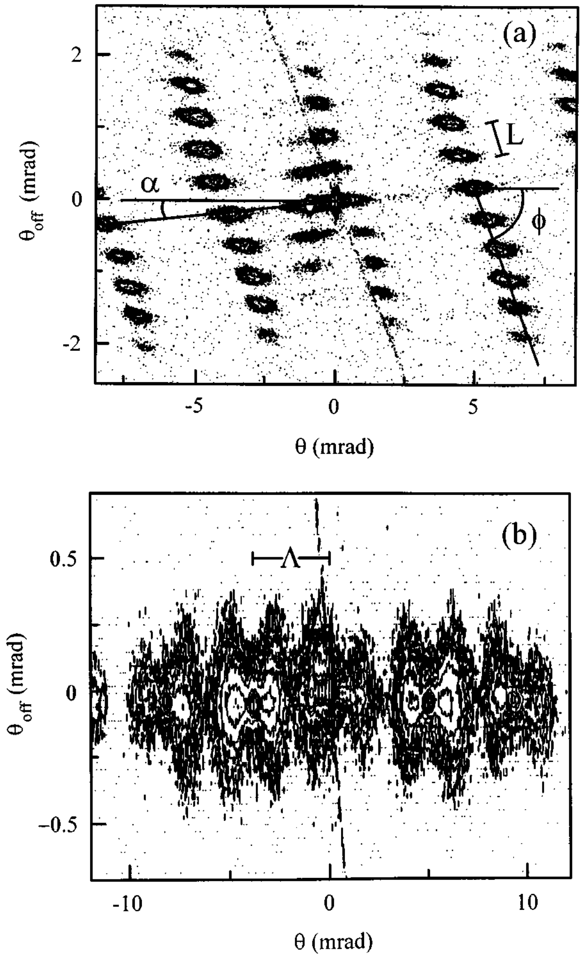

FIG. 3. High-angle RSM around the (004) rlp recorded on sample A for $\Psi=\pi/2$ rad (a) and $\Psi=0$ rad (b). Here, the azimuth angles $\Psi=\pi/2$ rad and $\Psi=0$ rad correspond to the measurement geometries of Figs. 2(a) and 2(b), respectively. The contour levels in the map (a) are at 2, 5, 8, 10, 25, 100, and 1000 counts/sec and in (b) are at 1.5, 3, 5, 10, 25, 50, 100, and 1000 counts/sec.

peaks is always equal and corresponds to the periodicity Λ. A possible explanation of this multiple peak distribution is that the actual unit cell can be considered to be formed by four distinct subcells as depicted in Fig. 4(c). This peculiar configuration of the unit cell is also suggested by the results of transmission electron microscopy analyses.[10] Each subcell is characterized by a certain lattice strain and dimension (layer thickness) even if the total thickness is always Λ.

Curve b in Fig. 5 shows the best simulation of the experimental profile obtained by using the dynamical theory of x-ray diffraction for distorted crystals.[12] The strain and thickness of each layer, as found from the simulation, are given in Table II. The results of this simulation provide further fundamental insight into the structure of the superlattice. The deformation within the epilayer unit cell changes laterally from a tensile (subcell I) to a compressive strain (subcells II, III, and IV). It is this lateral strain modulation which causes the appearance of the ''in-plane'' satellite peaks well observed in the RSM of Fig. 3.

B. Low-angle RSM, XSR, and XDS measurements

In order to inspect the interface roughness and the roughness correlation among the multilayer interfaces we per-

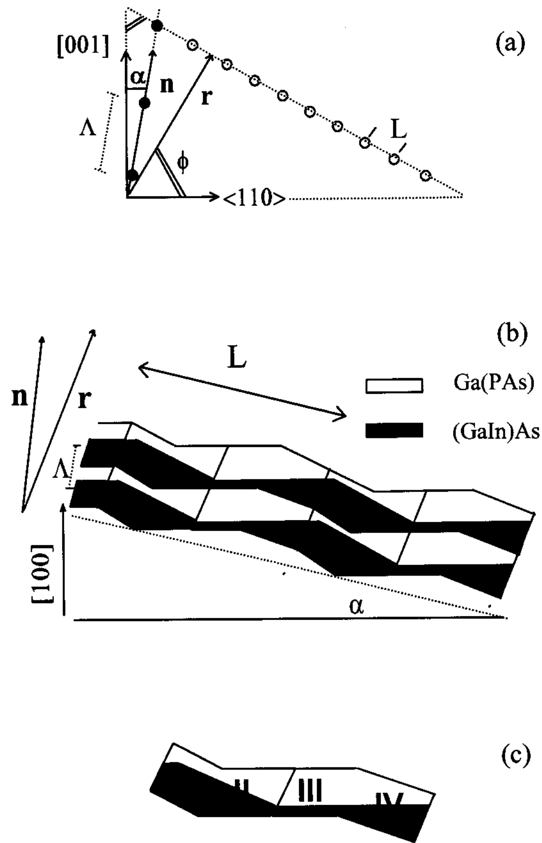

FIG. 4. Schematic description of the multilayer structure in the reciprocal space (a) and in the real space (b), respectively. The full and open circles correspond to the vertical and lateral satellite peaks. L and Λ are the lateral and vertical periodicities, **n** is the surface normal, **r** is the vector along the macrosteps developing direction, α is the angle between **n** and the [001] direction, ϕ the angle between **r** and the [110] direction. The actual unit cell (c) of the heterostructure is formed by four distinct subcells.

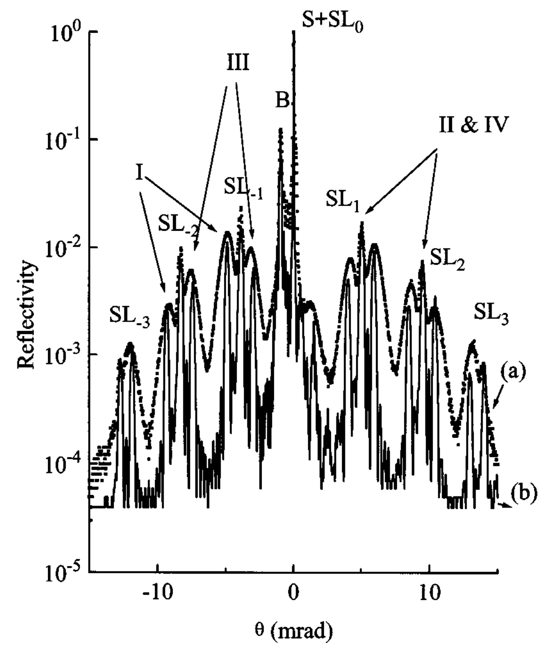

FIG. 5. Experimental (a) and simulated (b) HRXRD profiles of sample A measured in the vicinity of the (004) rlp at $\Psi=0$ rad. The simulated curve has been obtained considering the unit cell structure of Fig. 4(c) and the parameters given in Table II.

formed low-angle RSM, XSR, and XDS measurements on all the investigated samples. In this section we will focus our attention on the experimental results of sample A and we will analyze and discuss the obtained data in detail.

Figures 6(a) and 6(b) show the low-angle RSM measured on sample A in the vicinity of the (000) rlp for the azimuthal orientations $\Psi=\pi/2$ rad and $\Psi=0$ rad, respectively. A comparison between the two contour maps clearly indicates the strong anisotropy of the roughness distribution. If the sample is oriented with the macrosteps perpendicular to the scattering plane [Fig. 6(a)], the intensity distribution shows a vertical periodicity (coincident with Λ) along the specular reflectivity direction ($\theta_{\mathrm{off}}=0$ mrad) and a lateral periodicity (L_x) along each tranverse scan. The distribution of the diffuse intensity contains information about the lateral correlation between the steps and the vertical correlation between the (GaIn)As/Ga(PAs) interfaces.[17–19] In particular, the lateral correlation can be directly inspected by diffuse scattering in tranverse scan measurements, while the vertical correlation is measured by recording longitudinal scans (off-specular reflectivity measurements). Several tranverse scans corresponding to different Q_z values versus the in-plane component of scattering vector (Q_x) are reported in Fig. 7(a). The lateral periodicity ($L_x=320\pm20$ nm), which can be determined from the equispaced satellite peaks, coincides, within the error, with the value (L) determined from the high-angle RSM. The presence of higher-order diffuse satellite peaks indicates that the laterally correlated interface morphology is not pure sinusoidal.[16]

If the sample is oriented with the macrosteps parallel to the scattering plane [Fig. 6(b)] the intensity distribution depends on the vertical correlation between the heterointerfaces and on the lateral waviness along the macrosteps. Also in this case, we recorded single transverse scans at different Q_z positions, which are shown in Fig. 7(b) versus the Q_x vector. Two weak satellite peaks can be detected on both sides of the diffuse intensity that indicate the presence of a sinusoidal waviness along the macrosteps. The mean spatial wavelength of this roughness is $L_y=970\pm100$ nm, as determined from the distance between the satellites. Furthermore, the diffuse scattering is off-centered with respect to the specular peak, indicating a vertical correlation direction slightly off-oriented with respect to the growth direction.[16,17] A good vertical correlation between interfaces can be determined at this azimuthal orientation if the specular and off-specular reflectivity curves shown in Fig. 8 are compared. In fact, the longitudinal scan (curve b) shows a diffuse pattern that contains the same features of the specular reflectivity profile (curve a).

The structural analysis of the low-angle x-ray results can be summarized as follows. The morphology of the roughness on the growth surface is greatly influenced by the presence of the substrate miscut, i.e., by the strain-induced macrosteps. In particular, the roughness is laterally strongly replicated along the miscut direction following exactly the macrostep distance. Actually, the roughness has a two-dimensional distribution with a sinusoidal component also along the macrosteps. The two mean wavelengths of the roughness, as de-

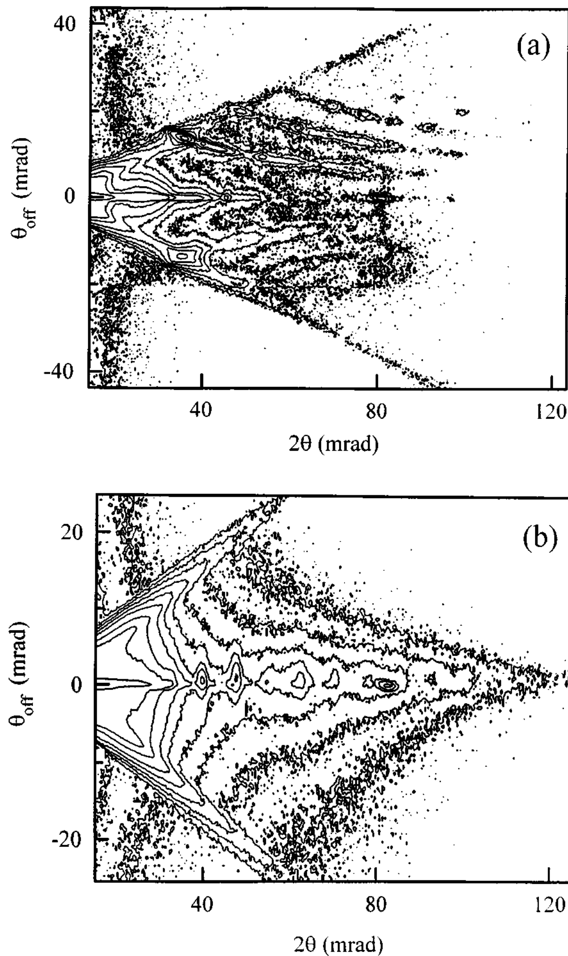

FIG. 6. Low-angle RSM recorded on sample A in the vicinity of the (000) rlp for the azimuthal orientations $\Psi=\pi/2$ rad (a) and $\Psi=0$ rad (b). Here, the azimuth angles $\Psi=\pi/2$ rad and $\Psi=0$ rad correspond to the measurement geometries of Figs. 2(a) and 2(b), respectively. The contour levels for both maps are at 6, 12, 25, 50, 100, 200, 500, 1000, and 10 000 counts/sec.

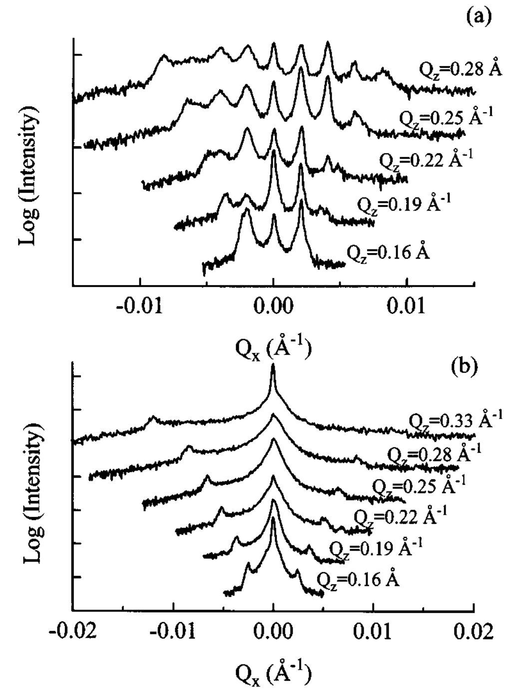

FIG. 7. XDS scans measured for different Q_Z on sample A for the azimuthal orientations $\Psi=\pi/2$ rad (a) and $\Psi=0$ rad (b). Here, the azimuth angles $\Psi=\pi/2$ rad and $\Psi=0$ rad correspond to the measurement geometries of Figs. 2(a) and 2(b), respectively. Pattern (a) exhibits several satellite peaks caused by the lateral periodicity.

termined from this structural analysis, are reported in Table III on sample A as well as on sample B.

Finally, we carefully investigated the surface morphology of these two samples by atomic-force microscopy in order to find any correlation occurring between surface and interface structural ordering.

C. AFM images

The surface topography and morphological features of the samples were investigated by atomic-force microscopy. Figure 9(a) shows an AFM image of a 9×9-μm^2 area of sample A. The AFM micrograph has been corrected by means of a calibration procedure using a reference grid[18] in order to eliminate any image distortion, which may be introduced during the acquisition, e.g., caused by the nonlinearity and/or memory effect of the PZT scanner. A periodic structure from left to right is clearly visible in Fig. 9(a), which is also evidenced by the presence along the x direction of satellite peaks in the two-dimensional Fourier transform (FT) of the image [see Fig. 9(b)]. The presence of a surface periodicity

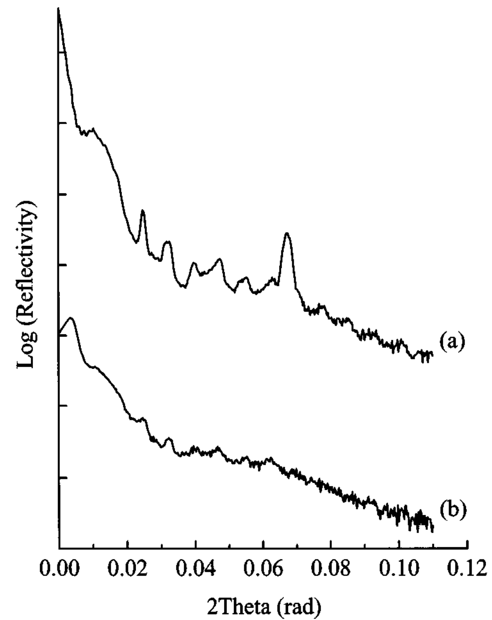

FIG. 8. Specular (a) and off-specular (b) scans on sample A for the azimuthal orientations $\Psi=0$ rad. The off-specular curve is measured at an offset angle of 4.4 mrad. Besides one peak belonging to the (AlGa)As/GaAs superlattice buffer layer ($2\theta=0.067$ rad) the off-specular scan shows still a tiny memory of the specular peaks measured in curve a. This indicates the presence of a vertical correlation among the interfaces of the (GaIn)As/Ga(PAs) multilayer.

TABLE III. The mean spatial wavelength (L_x and L_y) of the interface and surface roughness as determined by XDS measurements and atomic-force microscopy.

	X-ray		AFM	
Sample	L_x (nm)	L_y (nm)	L_x (nm)	L_y (nm)
A	320±10	970±120	350±20	1080±170
B	265± 5	850± 80	255±12	895±115

also in the other orthogonal direction (y direction) is not immediately evident in the AFM image as well as in the two-dimensional FT.

However, integrating the FT along the two orthogonal directions x and y, the curves of Fig. 10 are obtained and both clearly show the presence of satellite peaks. The FT integrated along the y direction (dotted curve) exhibits only two satellite peaks, indicated by the dotted arrow, in accordance with a single periodicity along the x axis (L_x). On the other hand, the FT integrated along the x direction (continuous curve) presents two *pairs* of satellites peaks, indicated by the solid-line arrows. The peaks close to the main maximum are just the projection along the y axis of L_x. This can be easily explained by the fact that the fringes of Fig. 9(a) are not exactly parallel to the y direction. However, the other pair of satellite peaks is actually due to a surface periodicity along the y direction (L_y), which is less regular with respect to that in the x direction and which is only slightly visible in the AFM image [Fig. 9(a)]. The lateral periodicities L_x and L_y measured from the integrated FT of the AFM images on samples A and B are reported in Table III together with the mean wavelengths determined from low-angle x-ray results. It should be noted that an excellent agreement between the ''internal'' lateral periodicity of the superlattice measured by XDS and RSM and the periodicity revealed on the samples surface by AFM is obtained.

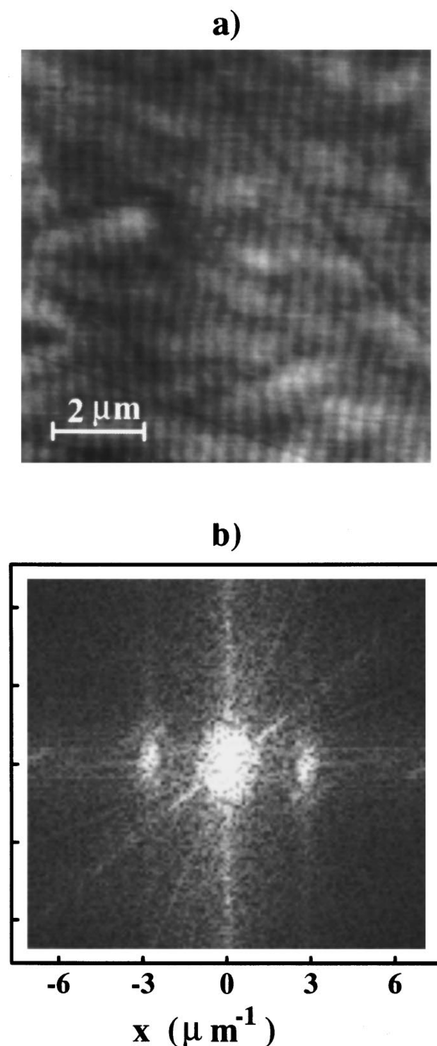

FIG. 9. Undistorted AFM image (a) of a 9×9-μm^2 area of sample A, corrected by calibration procedure using a reference grid. The Fourier transform (b) of the AFM image.

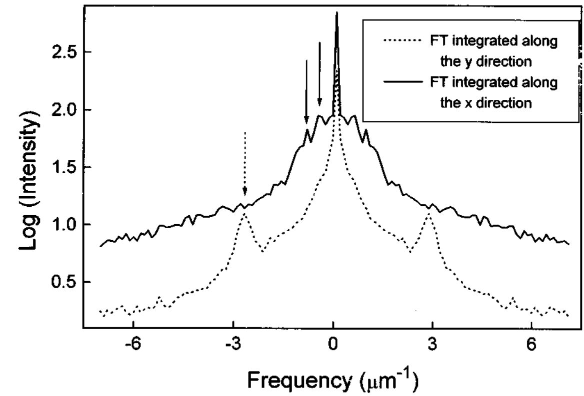

FIG. 10. The Fourier transform, shown in Fig. 9(b), integrated along the y direction (dotted curve), and along the x direction (solid curve). The two curves are shifted with respect to each other in order to evidence their particular features clearly. The dotted-line arrow indicates the satellite peak of the dotted curve, which is attributed to the periodicity along the x direction. The solid curve exhibits satellite peaks too, indicated by the solid-line arrows.

V. DISCUSSION

The successful growth of lateral superlattices on vicinal substrates has been already reported for tilted,[19,20] fractional-layer,[21] and serpentine[22] superlattices. In these cases, the lateral periodicity (about 10 nm) was directly determined by the monolayer steps occurring along the substrate surface because of the miscut angle. Besides the miscut of the substrate, the peculiarity of our structures is that the superlattice is composed of highly strained layers of opposite strain (tensile and compressive). In fact, from our experimental findings a much higher lateral period was measured, demonstrating that the formation of the macrosteps cannot be *only* attributed to the off-orientation of the substrate. A combined effect has to be invoked in order to explain such a large and regular periodicity. The second important result of our analyses is the strain distribution found in the epilayer unit cell (Table II). The presence of multiple satellite peaks in the HRXRD spectra (Fig. 5) evidences the lateral strain modulation within the cell going from a tensile strain in the subcell I to compressive strains in the subcells II, III, and IV. This epilayer unit cell is repeated periodically with a lateral periodicity of about 200–300 nm in correspondence to the

macrostep distance. Consequently, an irregularly shaped periodic profile of the interface is expected, as the roughness depends on the sign of the strain.[6] In fact, our data reveal the presence of a laterally correlated interface roughness with a mean spatial wavelength exactly equal to the macrostep periodicity and with a nonsinusoidal shape of the profile. The interface profile is more regular (sinusoidal) as found from the measurements performed when the sample is oriented with the macrosteps lying parallel to the scattering plane. Therefore, this semiquantitative analysis of our data gives already evidence of a close relationship between the interface profile and the strain distribution. In order to obtain a better understanding of this relationship and to clarify the experimental evidences, further work is necessary. In particular, a correct simulation the XSR, XDS, and low-angle RSM measurements is required in order to determine the correlation function that best describes the roughness profile of the different interfaces and to draw the actual shape of the macrosteps. This work is now in progress.

Finally, the AFM data and the low-angle x-ray results summarized in Table III allow us to draw a further important conclusion. In fact, the very good agreement of these values indicates that the ''internal'' interface ordering, as determined by the x-ray measurements, remains preserved up to the outer surface monitored by AFM observations. The finding of the same lateral periodicities throughout all the interfaces up to the surface is the fingerprint of an enhanced vertical correlation of the roughness within the whole multilayer thickness.

VI. CONCLUSIONS

We investigated the structural properties of symmetrically strained (GaIn)As/Ga(PAs) superlattices grown on off-oriented (001) GaAs substrates by means of high-resolution x-ray scattering techniques. In addition to the vertical periodicity along the growth direction we found a strained-induced reorganization of the multilayers that results in a highly periodic lateral structure (equispaced macrosteps).

Within the epilayer unit cell, our data show a characteristic lateral distribution of the strain going from tensile to compressive deformation zones. Therefore, a periodic lateral deformation with a mean distance of few hundreds of a nanometer (macrosteps distance) occurs. The interface roughness analyses reveal a laterally correlated two-dimensional roughness with a spatial wavelength corresponding exactly to the macrosteps distance and, in addition, another spatial wavelength along the macrosteps. Furthermore, a strong vertical correlation of the roughness explains the preserved interface ordering found up to the surface.

ACKNOWLEDGMENTS

The authors would like to thank Alberto Sacchetti and Laura Capodieci for the valuable technical support in x-ray and AFM measurements. One of us (Y.Z.) is greatful to the INFM, Genova (Italy) for the financial support. Part of this work has been supported by the Deutsche Forschungsgemeinschaft (DFG).

*Permanent address: Institute of Semiconductors, Chinese Academy of Sciences, Beijing 100083, China.

[1] D. J. Eaglesham and M. Cerullo, Phys. Rev. Lett. **64**, 1943 (1990).

[2] C. W. Snyder, B. G. Orr, D. Kessler, and L. M. Sander, Phys. Rev. Lett. **66**, 3032 (1991).

[3] C. W. Snyder, J. F. Mansfield, and B. G. Orr, Phys. Rev. B **46**, 9551 (1992).

[4] A. J. Pidduck, D. J. Robbins, A. G. Cullis, W. Y. Leong, and A. M. Pitt, Thin Solid Films **222**, 78 (1992).

[5] C. W. Snyder, B. G. Orr, and H. Munekata, Appl. Phys. Lett. **62**, 46 (1993).

[6] Y. H. Xie, G. H. Gilmer, C. Roland, P. J. Silverman, S. K. Buratto, J. Y. Cheng, E. A. Fitzgerald, A. R. Kortan, S. Schuppler, M. A. Marcus, and P. H. Citrin, Phys. Rev. Lett. **73**, 3006 (1994).

[7] A. Ponchet, A. Rocher, J.-Y. Emery, C. Starck, and L. Goldstein, J. Appl. Phys. **74**, 3778 (1993).

[8] A. Ponchet, A. Rocher, A. Ougazzaden, and A. Mircea, J. Appl. Phys. **75**, 7881 (1994).

[9] T. Marschner, S. Lugten, M. Volk, W. Stolz, E. O. Göbel, N. Y. Jin-Phillipp, and F. Phillipp, Superlattices Microstruct. **15**, 183 (1994).

[10] T. Marschner, L. Tapfer, N. Y. Jin-Phillipp, F. Phillipp, S. Lutgen, M. Volk, W. Stolz, and E. O. Göbel, Solid-State Electron. **40**, 819 (1996).

[11] P. F. Fewster, Semicond. Sci. Technol. **8**, 1915 (1993).

[12] L. Tapfer, in *III-V Quantum System Research*, edited by K. H. Ploog (The Institution of Electrical Engineering, Herts, UK, 1995), Chap. 8, pp. 225–260.

[13] Z. H. Ming, A. Krol, Y. L. Soo, Y. H. Kao, J. S. Park, and K. L. Wang, Phys. Rev. B **47**, 16 373 (1993).

[14] Y. H. Phang, D. E. Savage, R. Kariotis, and M. G. Lagally, J. Appl. Phys. **74**, 3181 (1993).

[15] D. E. Savage, J. Kleiner, N. Schimke, Y. H. Phang, T. Jankowski, J. Jacobs, R. Kariotis, and M. G. Lagally, J. Appl. Phys. **69**, 1411 (1991).

[16] Y. H. Phang, C. Teichert, M. G. Lagally, L. J. Peticolos, J. C. Bean, and E. Kasper, Phys. Rev. B **50**, 14 435 (1994).

[17] R. L. Headrick, J. M. Baribeau, and Y. E. Strausser, Appl. Phys. Lett. **66**, 96 (1995).

[18] L. De Caro, M. F. De Riccardis, and L. Tapfer (unpublished).

[19] J. M. Gaines, P. M. Petroff, H. Kroemer, R. J. Simes, R. S. Geels, and J. H. English, J. Vac. Sci. Technol. B **6**, 1378 (1988).

[20] S. A. Chalmers, A. C. Gossard, and H. Kroemer, Appl. Phys. Lett. **57**, 1751 (1990).

[21] T. Fukui, H. Saito, and Y. Tokura, Jpn. J. Appl. Phys. **27**, L1320 (1988).

[22] M. Krishnamurthy, M. S. Miller, and P. M. Petroff, Appl. Phys. Lett. **61**, 2990 (1992).